

# Probing nearest-neighbor correlations of ultracold fermions in an optical lattice

Daniel Greif, Leticia Tarruell,\* Thomas Uehlinger, Robert Jördens, and Tilman Esslinger  
*Institute for Quantum Electronics, ETH Zurich, 8093 Zurich, Switzerland*

(Dated: February 16, 2022)

We demonstrate a probe for nearest-neighbor correlations of fermionic quantum gases in optical lattices. It gives access to spin and density configurations of adjacent sites and relies on creating additional doubly occupied sites by perturbative lattice modulation. The measured correlations for different lattice temperatures are in good agreement with an *ab initio* calculation without any fitting parameters. This probe opens new prospects for studying the approach to magnetically ordered phases.

PACS numbers: 03.75.Ss, 05.30.Fk, 71.10.Fd, 78.47.-p

The Fermi-Hubbard Hamiltonian is one of the central models for understanding strongly correlated electron systems in condensed matter physics. It incorporates intriguing phenomena such as Mott-insulating behavior or spin ordered phases and is a prominent candidate for describing the origin of high  $T_c$  superconductivity. Despite tremendous theoretical effort, several questions still remain open, in particular concerning the low temperature phases. Here, ultracold atomic gases trapped in optical lattices offer the opportunity to address these questions in a very clean way, as they constitute an almost ideal implementation of the Hubbard model [1, 2]. The recent realization of a fermionic Mott insulator [3, 4] demonstrates the unique tunability and control of these systems.

Considerable experimental efforts are currently directed towards reaching the low-temperature regime of quantum magnetism in a two-component quantum gas. Detection of the antiferromagnetically ordered state has been proposed via noise correlation or Bragg scattering measurements [5, 6]. These observables reveal long range spin ordering and consequently only show a strong signature well below the critical temperature. However, a probe sensitive to local magnetic correlations [7, 8] for studying the approach to magnetic ordering of fermions close to the transition point is missing so far.

In this Letter we demonstrate a simple method for probing the nearest-neighbor correlations of strongly interacting repulsive fermionic gases in optical lattices. The correlation function is given by

$$\mathcal{P}_{i,i+1} = \sum_{\sigma} \langle n_{i,\sigma} n_{i+1,\bar{\sigma}} (1 - n_{i,\bar{\sigma}}) (1 - n_{i+1,\sigma}) \rangle, \quad (1)$$

where  $\sigma = \{\uparrow, \downarrow\}$ ,  $\bar{\sigma}$  are opposite spins and  $i, i+1$  adjacent sites. This probe determines the probability of finding singly occupied neighboring sites with opposite spins.

The experimental strategy for detecting the correlator  $\mathcal{P}_{i,i+1}$  relies on exciting the system by a periodic modulation of the lattice depth [9]. The corresponding modulation in kinetic energy leads to tunneling of particles to adjacent sites. If two particles of opposite spin are located on neighboring sites, additional double occupancies (doublons) are created as shown in Fig. 1. The resulting dou-

blon production rate is sensitive on the nearest-neighbor density and spin correlator  $\mathcal{P}_{i,i+1}$ . In the following we describe and characterize this experimental method and show that in the perturbative regime the frequency integrated doublon production rate is given by  $\mathcal{P}_{i,i+1}$  [10–13]. We then use this technique to measure nearest-neighbor correlations as a function of temperature covering the regime from a paramagnetic Mott insulator to a strongly interacting metallic state. The results are in good agreement with the predictions of an *ab initio* theory without any fitting parameters.

The experimental sequence used to produce a quantum degenerate Fermi gas has been described in detail in previous work [14, 15]. In brief, a balanced spin mixture of  $^{40}\text{K}$  atoms in the  $m_F = -9/2$  and  $-5/2$  magnetic sublevels of the  $F = 9/2$  hyperfine manifold is evaporatively cooled in an optical dipole trap. For samples of  $N = 80(7) \times 10^3$  atoms we reach temperatures as low as 14% of the Fermi temperature  $T_F$ . Subsequently we ramp up a three-dimensional optical lattice of simple cubic geometry and lattice constant  $d = 532$  nm. The lattice depth is increased in 0.2 s to final values of  $7.0(7) E_R$  or  $10(1) E_R$ , where  $E_R = \hbar^2/8md^2$  is the recoil energy,  $\hbar$  is Planck's constant and  $m$  denotes the mass of  $^{40}\text{K}$ . The

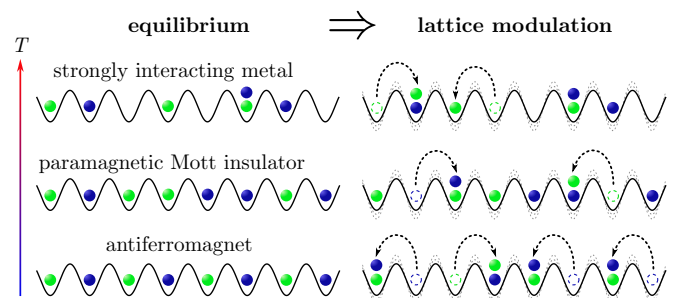


FIG. 1: (color online) Probing nearest-neighbor correlations for different phases. A periodic lattice modulation causes tunneling of particles to neighboring sites. The number of created doublons strongly depends on the state of the many-body system (strongly interacting metal, paramagnetic Mott insulator or antiferromagnet) and can be used to determine the nearest-neighbor correlator  $\mathcal{P}_{i,i+1}$  [10].

hopping  $t$  is inferred from Wannier functions [16] and the on-site interaction energy  $U$  is obtained from lattice modulation spectroscopy [3]. The underlying trapping potential has a mean frequency of  $\omega/2\pi = 70.1(5)$  Hz for  $7 E_R$  and  $\omega/2\pi = 77.3(7)$  Hz for  $10 E_R$ . With this procedure we create samples where the core is in the Mott insulating regime [15].

After this preparation, the lattice depth is modulated by  $\delta V$  along all three axes in time  $\tau$  according to  $V(\tau) = V + \delta V \sin(2\pi\nu\tau)$ . This results in a modulation of both the hopping and the on-site interaction with amplitudes  $\delta t$  and  $\delta U$  respectively, creating additional doubly occupied sites as compared to the initial state. The increase in the number of doublons is maximal when the modulation frequency  $\nu$  coincides with the doublon energy (resonant excitation at  $\nu = U/h$ ). After the lattice modulation, the fraction of atoms on doubly occupied sites  $D = 2 \sum_i \langle n_{i,\uparrow} n_{i,\downarrow} \rangle / N$  is measured by mapping doublons into a different spin state, subsequent Stern-Gerlach separation and absorption imaging [3].

Fig. 2 (a) shows the evolution of double occupancy as a function of lattice modulation time for resonant excitation. After a steep initial rise, we observe a saturation of

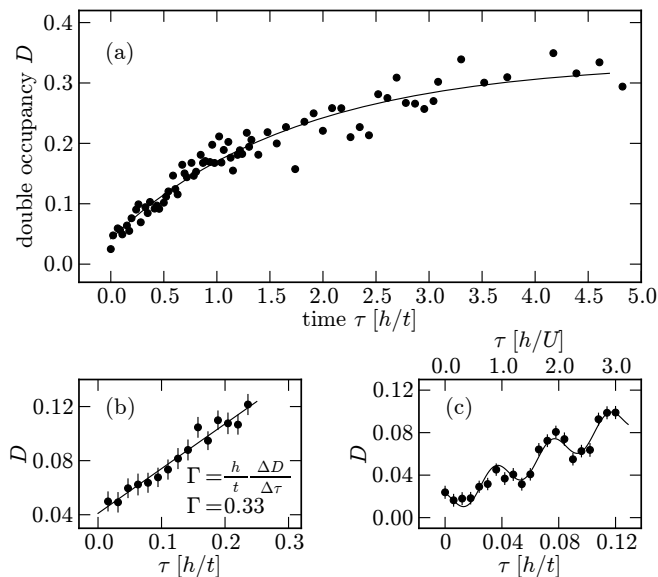


FIG. 2: Evolution of double occupancy as a function of the lattice modulation time  $\tau$  for resonant excitation. The lattice depth is set to  $7 E_R$  ( $U/6t = 4.1$ ) and the modulation strength is  $\delta V/V = 0.1$ . (a) The induced double occupancy saturates for large times, which is well captured by an exponential fit (solid line). (b) At low modulation times  $D$  increases linearly, from which the doublon production rate  $\Gamma$  is obtained by a linear fit. The lattice depth was set to  $10 E_R$  for this measurement ( $U/6t = 10.6$ ). (c) On the timescale of the modulation period  $h/U$  the double occupancy shows an underlying low amplitude sinusoidal modulation. The solid line is a fit with fixed frequency  $U/h$ . For clarity,  $\delta V/V$  was increased to 0.2. Error bars in double occupancy denote statistical errors from multiple measurements.

the induced double occupancy on a timescale on the order of the tunneling time  $h/t$ . The saturation value depends only weakly on the modulation strength and reaches typical values of 20 – 30%. In contrast to previous work, where only this saturation regime was considered [3, 14], our high accuracy in the determination of double occupancy allows us to perform measurements in the weak excitation limit. Here we find that double occupancy increases linearly with time as shown in Fig. 2(b). We extract the normalized doublon production rate  $\Gamma$  from the slope  $\Delta D/\Delta\tau$  of a linear fit to the data

$$\Gamma = \frac{h}{t} \frac{\Delta D}{\Delta\tau}. \quad (2)$$

On shorter timescales an underlying oscillatory response at the modulation frequency  $\nu$  is observed, Fig. 2(c).

The experiment can be well understood in the framework of time-dependent perturbation theory, which we outline below. The main result is that the frequency integrated doublon production rate is proportional to the nearest-neighbor correlator  $\mathcal{P}_{i,i+1}$ . The Hamiltonian of the system can be written as  $H = H_0 + H_{\text{pert}}(\tau)$ , where  $H_0 = -tH_t + UH_U$  is the Fermi-Hubbard Hamiltonian and the time-dependent perturbation is given by  $H_{\text{pert}}(\tau) = (\delta t H_t + \delta U H_U) \sin(2\pi\nu\tau)$ . Assuming that the doublon production rate is equivalent to the total energy absorption rate (which becomes exact at half-filling and  $U \gg t$ ), the perturbation in  $U$  can be mapped to an increased tunneling perturbation with amplitude  $\tilde{\delta}t/t = \delta t/t - \delta U/U$  [17]. The response of the system to second order in perturbation theory is then given by

$$D(\tau) = D(0) + \left(\frac{\tilde{\delta}t}{t}\right) \chi^{(1)}(\nu) \sin(2\pi\nu\tau) + \left(\frac{\tilde{\delta}t}{t}\right)^2 \left[ \chi^{(2)}(\nu) \frac{\tau}{h/t} + \text{osc. terms} \right], \quad (3)$$

in good agreement with the experimental observations of Fig. 2 (b),(c) using  $\Gamma = \chi^{(2)}(\nu)(\tilde{\delta}t/t)^2$ . The susceptibilities  $\chi^{(1)}(\nu)$  and  $\chi^{(2)}(\nu)$  correspond to the linear response and the non-oscillatory part of the quadratic response respectively. This is recovered by Fermi's Golden Rule

$$\chi^{(2)}(\nu) = \frac{2\pi^2 t}{Nh} \sum_n \langle n | \delta H_U | n \rangle |\langle n | H_t | 0 \rangle|^2 \delta(\nu - \nu_{n0}).$$

Here  $|0\rangle$  and  $|n\rangle$  denote the unperturbed and excited states of  $H_0$ ,  $h\nu_{n0}$  is their energy difference and  $\delta H_U$  counts the number of additionally created doublons [11]. Evaluating all contributing matrix elements in the limit  $U \gg t$ , the sum over all excited states is then equal to  $\mathcal{P}_{i,i+1}$ . To compare with experiments we consider the normalized frequency integrated response

$$R = \frac{h}{U} \int d\nu \Gamma(\nu) = 2\pi^2 \left(\frac{\tilde{\delta}t}{t}\right)^2 z \frac{t}{U} \mathcal{P}, \quad (4)$$

where  $\mathcal{P} = \sum_i \mathcal{P}_{i,i+1}/N$  is the system averaged correlator and  $z$  the connectivity of the lattice. In the perturbative regime  $R$  therefore gives direct access to the nearest-neighbor correlator  $\mathcal{P}$  of the unperturbed initial state.

We validate that the experiments are performed in the weak excitation regime by studying the scaling of  $R$  with the relative modulation amplitude  $\tilde{\delta}t/t$  [24]. We measure the doublon production rate as a function of the modulation frequency, from which the modulation spectra in Fig. 3 are obtained. The frequency integrated response is then determined by a gaussian fit to each spectrum. The result is plotted as a function of the lattice modulation amplitude  $\tilde{\delta}t/t$  (inset of Fig. 3). We find a scaling exponent of 2.09(18), in very good agreement with the expected value of 2 predicted by second order perturbation theory. We can thus infer the nearest-neighbor correlator  $\mathcal{P}$  from the frequency integrated response.

Further information can be obtained from the lineshape of the modulation spectra, which reveals the density of states of the excitations. At half filling and temperatures well above the Néel transition, the density of states has an approximately triangular shape of full width  $\sim 3zt$  [12]. However, the trapping potential is expected to broaden the spectrum and introduce deviations to the lineshape [10]. This is consistent with the experimental data, which is well captured by gaussian fits with  $1/e^2$  diameters of  $4zt$ . The doublon production rate on resonance shows the same scaling behavior as the integrated response  $R$ , with a scaling exponent of 1.98(11). This allows us to determine  $\mathcal{P}$  from the resonant doublon production rate alone assuming a gaussian density of states as in Fig. 3 [25].

We now use doublon production rate measurements to determine the nearest-neighbor correlator  $\mathcal{P}$  as a function of entropy for  $U/6t = 4.1$ . We prepare samples with different entropies per particle by adding a variable waiting time in the optical dipole trap of up to 2s, which results in heating due to inelastic scattering processes. The entropy per particle  $s_{\text{in}}$  before loading into the lattice is inferred from Fermi fits to the momentum distribution of the cloud after expansion. This is a lower bound for the specific entropy in the lattice, as non-adiabatic processes take place during the loading. An upper bound  $s_{\text{out}}$  is given by the entropy measured after reversing the loading procedure.

The nearest-neighbor correlator rapidly decreases with increasing entropy, as shown in Fig. 4(a). This behavior has a simple physical interpretation: in a harmonically trapped lattice system higher temperatures lead to an increased cloud size, which results in a large number of empty sites. The probability of finding two neighboring singly occupied sites is therefore strongly reduced. This qualitative picture is confirmed by *ab initio* calculations of the nearest-neighbor correlator. We use a high temperature series expansion (HTSE) up to second order in

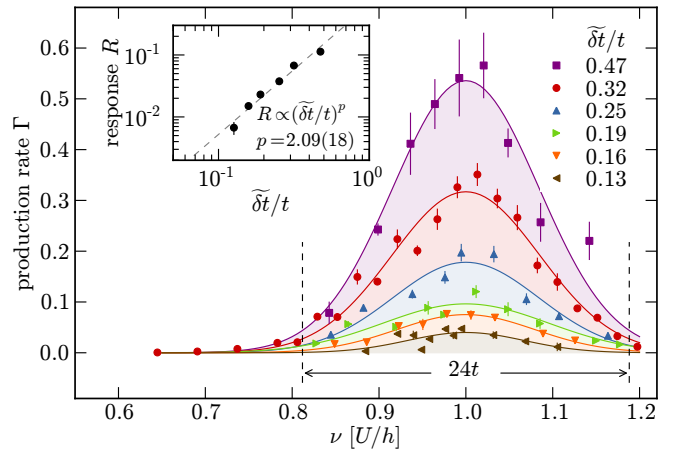


FIG. 3: (color online) Doublon production rate  $\Gamma$  as a function of the lattice modulation frequency  $\nu$ , measured for different modulation amplitudes  $\tilde{\delta}t/t$ . The experiments are performed at  $U/6t = 10.6$  and  $V = 10E_R$ . The shaded areas are gaussian fits to the spectra, which are used to extract the frequency integrated response  $R$ . The two vertical dashed lines denote twice the three-dimensional bandwidth  $4zt$  (with  $z = 6$ ). The inset is a double-logarithmic plot of  $R$  for various modulation amplitudes, where the dashed line is a power law fit. Error bars denote the fit errors.

$t/k_B T$ , where  $k_B$  is the Boltzmann constant [18, 19]. Due to the harmonic confinement, the trap averaged correlator  $\mathcal{P}$  needs to be evaluated. This is done using a local density approximation, which is an excellent assumption in this temperature regime [20]. The system parameters are calibrated by independent methods [15]. The results of this calculation are shown in Fig. 4(a).

We find quantitative agreement between the measured nearest-neighbor correlator and the theoretical predictions without any fitting parameters. The theoretical entropies  $s$  corresponding to the measured values of  $\mathcal{P}$  lie in between the lower and upper experimental bounds  $s_{\text{in}}$  and  $s_{\text{out}}$ . Nearest-neighbor correlation measurements thus allow us to determine entropy and temperature in the lattice for regimes where theory is still reliable and a quantitative comparison is possible. In contrast to thermometry in the optical dipole trap, the correlator  $\mathcal{P}$  is a direct observable in the lattice and does not rely on adiabaticity assumptions during the loading procedure. A comparison of these two methods suggests increased heating during the loading of the lattice for colder initial temperatures.

Further insight can be obtained from the theoretical model by investigating the spatial distribution of the nearest-neighbor correlator over the trap. From the inferred entropies  $s$  we calculate the profiles shown in Fig. 4(b) and (c) for the parameters of our system [26]. At half filling and deep in the Mott insulating regime  $\mathcal{P}_{i,i+1}$  is expected to be close to 0.5, whereas thermal excitations reduce this number in the metallic phase. This is

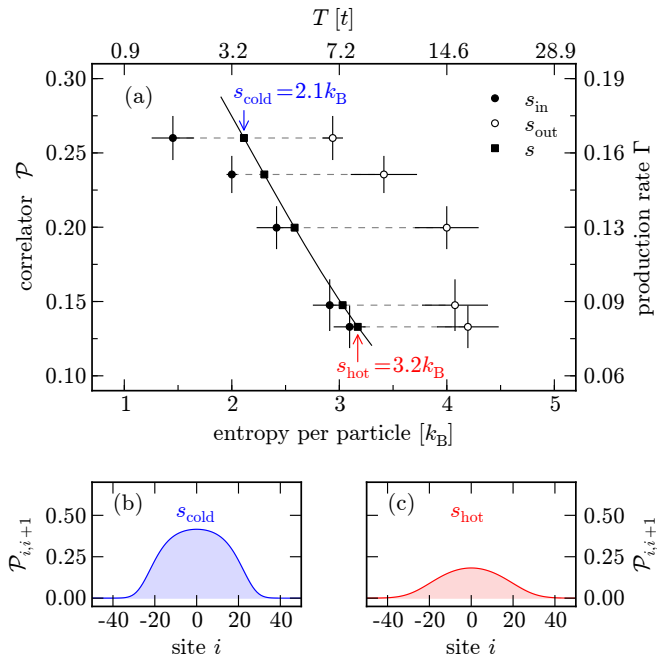


FIG. 4: (color online) Measurement of the nearest-neighbor correlator  $\mathcal{P}$ . (a) Dependence on entropy per particle in a trapped lattice system for  $U/6t = 4.1$ ,  $V = 7E_R$  and  $\tilde{\delta}t/t = 0.26$ . Solid and open circles denote lower and upper bounds  $s_{\text{in}}$  and  $s_{\text{out}}$  for the entropy per particle in the lattice for each measured value of  $\mathcal{P}$ . The black solid line is the calculated nearest-neighbor correlator obtained from second order HTSE without any fitting parameters. The entropy  $s$  inferred from comparing each measured value of  $\mathcal{P}$  to theory lies in between the experimental bounds. For clarity the corresponding lattice temperatures  $T$  and measured doublon production rates  $\Gamma$  are also included. Error bars denote statistical errors from several measurements. (b) and (c) show the calculated distribution of  $\mathcal{P}_{i,i+1}$  in the trap for the lowest and highest entropies  $s_{\text{cold}}$  and  $s_{\text{hot}}$ , while the area under these curves corresponds to the measured correlator  $\mathcal{P}$ .

confirmed by the values in the core of the system, with 0.44 for the coldest and 0.17 for the hottest point. The decrease in  $\mathcal{P}_{i,i+1}$  thus signals the transition from a paramagnetic Mott insulator to a strongly interacting metal. As the onset of local spin correlations corresponds to an increase of  $\mathcal{P}_{i,i+1}$  above 0.5, nearest-neighbor correlation measurements are a promising tool for studying the approach to the antiferromagnetic phase [22].

In conclusion, we have measured nearest-neighbor correlations of ultracold fermions in optical lattices by determining the response of the system to a weak lattice modulation. This observable is well suited for thermometry in the lattice and can be used to explore novel cooling schemes [21]. The technique opens new prospects for studying the approach to the antiferromagnetic phase, since the regime between a paramagnetic Mott insulator and an antiferromagnet is governed by the formation of short-range magnetic correlations. In the future,

nearest-neighbor correlation measurements might give insight into resonating valence bond ground states, where singlet correlations on neighboring sites are expected to occur in the absence of long range ordering [23].

We are grateful to N. Strohmaier and H. Moritz for contributions in the early stages of the experiment, and to G. Jotzu for a critical reading of the manuscript. We thank M. A. Cazalilla, E. Demler, T. Giamarchi, F. Hassler, A. Ho, S. Huber, C. Kollath, D. Pekker, L. Pollet, A. Rüegg, R. Sensarma and A. Tokuno for insightful discussions, and SNF, NCCR-MaNEP, NAME-QUAM (EU, FET open) and SQMS (ERC advanced grant) for funding.

\* Electronic address: tarruell@phys.ethz.ch

- [1] I. Bloch, J. Dalibard and W. Zwerger, *Rev. Mod. Phys.* **80**, 885 (2008).
- [2] T. Esslinger, *Ann. Rev. Cond. Mat. Phys.* **1**, 129 (2010).
- [3] R. Jördens *et al.*, *Nature (London)* **455**, 204 (2008).
- [4] U. Schneider *et al.*, *Science* **322**, 1520 (2008).
- [5] E. Altman, E. Demler and M. Lukin, *Phys. Rev. A* **70**, 013603 (2004).
- [6] T. A. Corcovilos *et al.*, *Phys. Rev. A* **81**, 013415 (2010).
- [7] S. K. Baur and E. J. Mueller, *Phys. Rev. A* **82**, 023626 (2010).
- [8] S. Trotzky *et al.*, *Phys. Rev. Lett.* **105**, 265303 (2010).
- [9] T. Stöferle *et al.*, *Phys. Rev. Lett.* **92**, 130403 (2004).
- [10] C. Kollath *et al.*, *Phys. Rev. A* **74**, 041604 (2006).
- [11] S. D. Huber and A. Rüegg, *Phys. Rev. Lett.* **102**, 065301 (2009).
- [12] T. Sensarma *et al.*, *Phys. Rev. Lett.* **103**, 035303 (2009).
- [13] F. Hassler and S. D. Huber, *Phys. Rev. A* **79**, 021607 (2009).
- [14] N. Strohmaier *et al.*, *Phys. Rev. Lett.* **104**, 080401 (2010).
- [15] R. Jördens *et al.*, *Phys. Rev. Lett.* **104**, 180401 (2010).
- [16] D. Jaksch *et al.*, *Phys. Rev. Lett.* **81**, 3108 (1998).
- [17] A. Reischl, K. P. Schmidt and G. S. Uhrig, *Phys. Rev. A* **72**, 063609 (2005).
- [18] D. F. B. ten Haaf and J. M. J. van Leeuwen, *Phys. Rev. B* **46**, 6313 (1992).
- [19] J. A. Henderson, J. Oitmaa and M. C. B. Ashley, *Phys. Rev. B* **46**, 6328 (1992).
- [20] V. W. Scarola *et al.*, *Phys. Rev. Lett.* **102**, 135302 (2009).
- [21] J. S. Bernier *et al.*, *Phys. Rev. A* **79**, 06160 (2009).
- [22] S. Fuchs *et al.*, *Phys. Rev. Lett.* **106**, 030401 (2011).
- [23] P. W. Anderson, *Science* **235**, 1196 (1987).
- [24] We use  $\tilde{\delta}t/t = -\sqrt{V/E_R}\delta V/V$ , which is accurate to a few percent for the lattice depths used in the experiment.
- [25] We have verified this assumption by inferring the value of the nearest-neighbor correlator from the inset of Fig. 3, which is in good agreement with the model.
- [26] The local value of the nearest-neighbor correlator is obtained by combining the HTSE result with a local density approximation. The average over all sites then yields the values of  $\mathcal{P}$  shown in Fig. 4(a).